

Channel cross-section heterogeneity of particulate organic carbon transport in the Huanghe

Yutian Ke^{1†}, Damien Calmels¹, Julien Bouchez², Marc Massault¹, Benjamin Chetelat³, Aurélie Noret¹, Hongming Cai², Jiubin Chen³, Jérôme Gaillardet², Cécile Quantin¹

¹GEOPS, Université Paris-Saclay-CNRS, 91405 Orsay, France

²Université de Paris, Institut de Physique du Globe de Paris, CNRS, 75005 Paris, France

³School of Earth System Science, Institute of Surface-Earth System Science, Tianjin University, 300072 Tianjin, China

[†]Present address: Division of Geological and Planetary Science, California Institute of Technology, Pasadena, CA 91125, USA

Corresponding author: Yutian KE (yutianke@caltech.edu)

Contents of this file

Section S1
Figures S1 to S7
Table S1

Introduction

This supporting material consists of 6 figures, 1 text and 1 table. Figure S1 presents the lithological map of the Huanghe drainage basin. Text S1 provides a detailed method description of constructing the velocity profile and of estimating the instantaneous suspended particulate matter (SPM) and particulate organic carbon (POC) flux over a channel cross-section. Figure S2 is the monthly water discharge and sediment flux recorded by three gauging stations (Huayuankou, Gaocun, and Lijin) in the lower Huanghe. Figure S3 gives the modeled spatial distribution of particle size (D₅₀), concentration and POC content of SPM. Figure S4 shows the particle size distribution of SPM samples collected in this study. Figure S5 gives a general idea of the well-correlation among physical and chemical parameters of SPM in the Huanghe. Figure S6 shows N/C_{org} variations in the Xifeng loess-paleosol sequence in the Chinese Loess Plateau in support of source determination in the main context. Figure S7 presents the mixing space of three POC end members for building the MixSIAR model. Table S1 provides the particles size D₁₀, D₅₀, D₉₀ parameters in Figure S4.

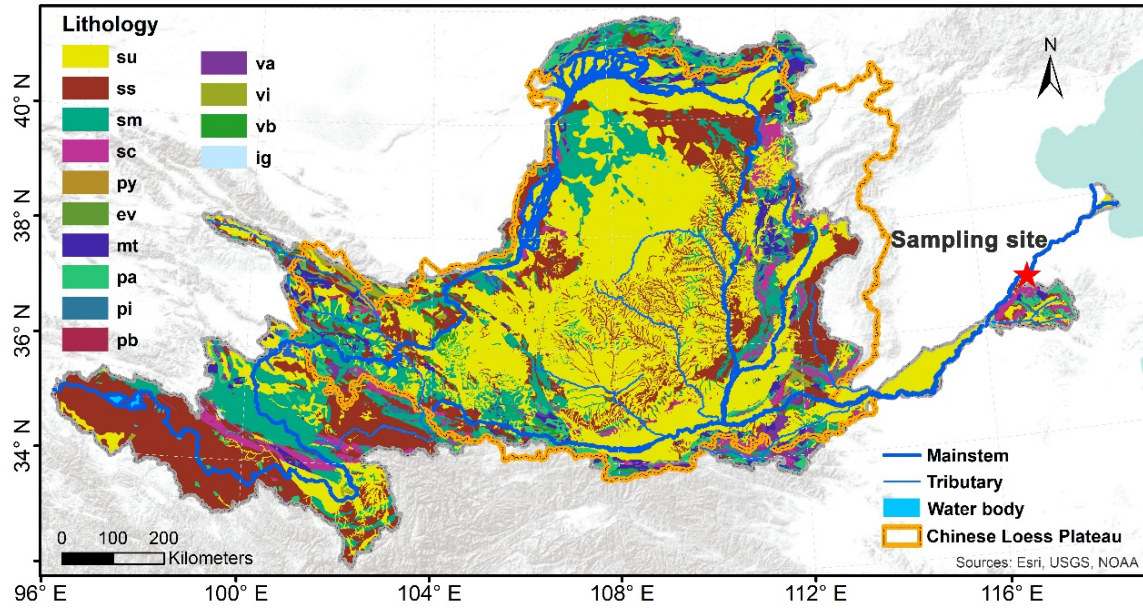


Figure S1: Lithological map of the Yellow River Basin (data extracted from the GLiM v1.1 database by Hartmann and Mossdorf, 2012). Except for no data (ND) and water body (wb), the lithology is as follows. su: Unconsolidated Sediments; ss: Siliciclastic Sedimentary Rocks; sm: Mixed Sedimentary Rocks; sc: Carbonate Sedimentary Rocks; py: Pyroclastics; ev: Evaporites; mt: Metamorphic Rocks; pa: Acid Plutonic Rocks; pi: Intermediate Plutonic Rocks; pb: Basic Plutonic Rocks; va: Acid Volcanic Rocks; vi: Intermediate Volcanic Rocks; vb: Basic Volcanic Rocks; ig: Ice and Glaciers. Figure is created using ESRI ArcGIS 10.3.

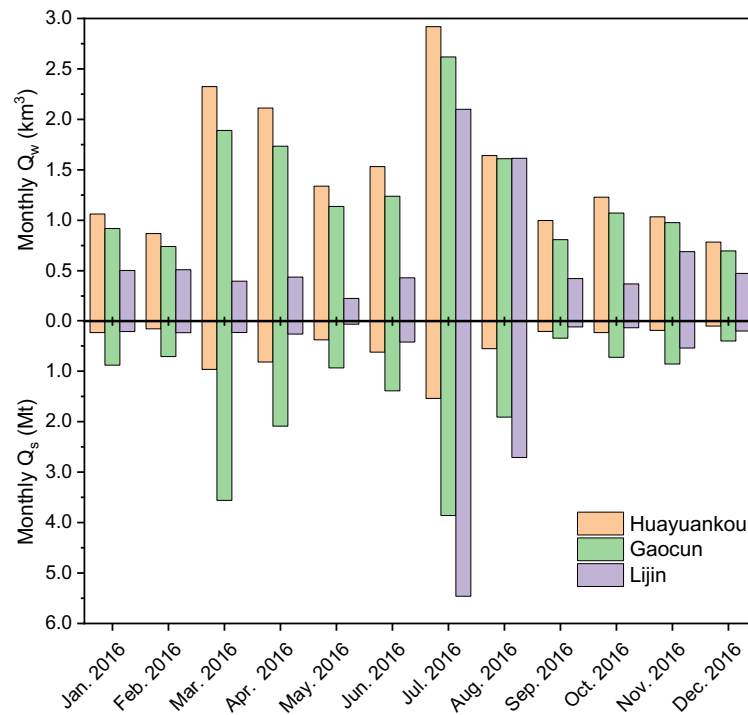


Figure S2: Monthly water discharge and sediment flux in the lower Huanghe in 2016. Hydrologic record is from three gauging stations (Huayuankou, Gaocun, and Lijin), data is available at <http://www.mwr.gov.cn>.

Section S1.

Sediment and POC flux estimation methods

We used water flow velocity profiles to “map” the flow velocity distribution across the river section. After constructing a bathymetric profile of the river cross-section based on the depth profiles, the flow velocity distribution across the river transect was modeled by the so-called velocity-defect law (Garcia, 2008) (Equation 1) which assumed that the maximum flow velocity u_{\max} takes place at the water surface *i.e.* at $z = H$.

$$\frac{u_{\max} - u}{u^*} = -\frac{1}{\kappa} \ln \frac{z}{H} \quad (1)$$

where z is the height above the riverbed, H is the channel depth, u^* is the bottom shear velocity and κ is the von Karman’s constant equal to 0.41.

Each velocity profile is fitted with the velocity-defect law and a pair of u_{\max} and u^* values are estimated. Values of these two parameters are then linearly interpolated between profiles to model the water velocity distribution across the river section. For profiles where only one velocity data was measured, we assumed that the velocity was constant with depth.

Variation of SPM concentrations with depth in large rivers can be described by a Rouse profile (e.g., Bouchez et al., 2011) where the Rouse model (Rouse, 1937) assumes that downward flux of sinking SPM is in equilibrium with the upward flux of SPM re-suspended from the riverbed due to turbulent flow. This model can be described by the following equation:

$$\frac{C(z)}{C(a)} = \left(\frac{H-z}{z} / \frac{H-a}{a} \right)^{Z_R} \quad (2)$$

where C is the SPM concentration, z is the height above the riverbed, a is a reference height above the riverbed, H is the channel depth, Z_R is the Rouse number. The surface sampling point was chosen as the reference height a in the Rouse equation. For each profile, the variation of the SPM concentration with depth is “fitted” by the Rouse equation which allows to determine the value of the Rouse number and then, to calculate the near-bottom sediment concentration. The Rouse equation is then used to model the distribution of the SPM concentration (Figure S3a) over the whole river cross section using a linear, lateral interpolation of the Rouse numbers and near-bottom concentration between profiles, and extrapolating from the lateral profiles to the corresponding riverbanks.

The Rouse equation can also be used to model the variations of the concentrations with depth for each individual class of grain size. For a given depth profile, each class of grain size shows a different “Rouse profile”. Fine particles show a more uniform distribution of concentration with depth (‘vertical profile’) characterized by a small Rouse number whereas coarse particles are concentrated near the bottom of the river and their concentration profile are characterized by a larger Rouse number. The calculation of the different classes of grain sizes allows for modeling the spatial distribution of D50 across the whole river transect (Figure S3b). Based on the relationships between D50 and Al/Si and between Al/Si and POC content, it is then possible to model the distribution of the Al/Si ratios and the POC content (Figure S3c) over the river section.

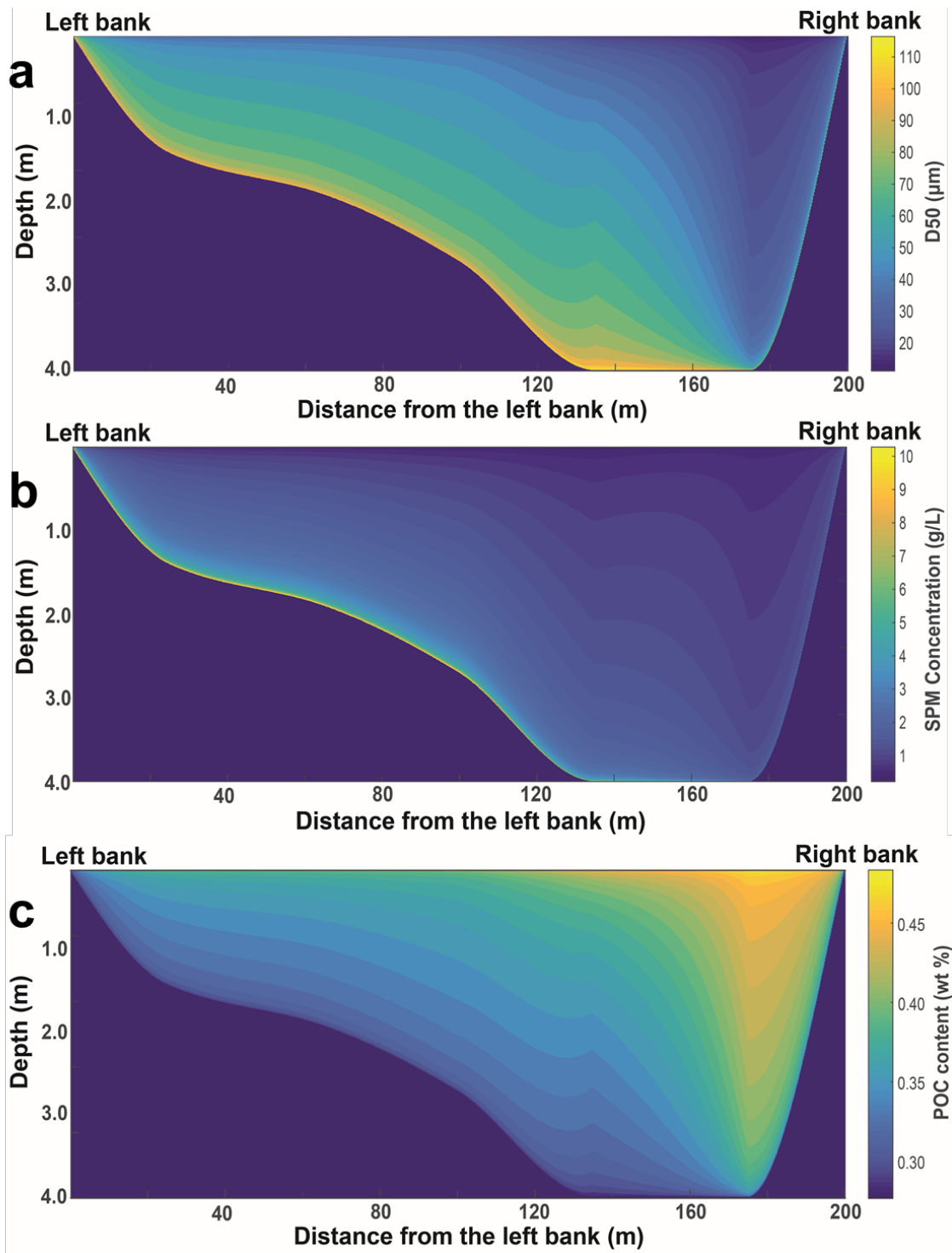


Figure S3: Modeled spatial distribution of (a) particle size (D50), (b) SPM concentration, and (c) POC content (%) over the channel cross section at Luokou.

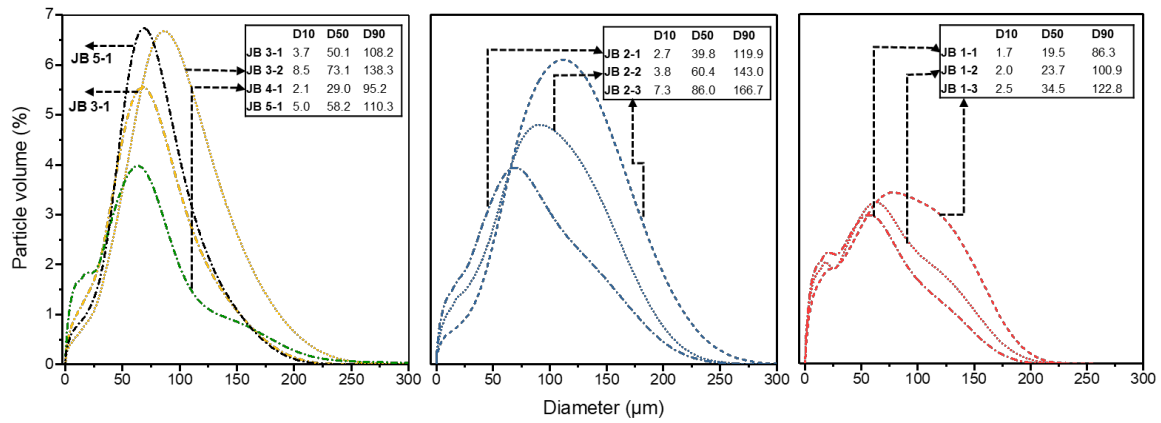


Figure S4. Particle size distribution of SPM over the channel cross section at Luokou. Particle size parameters including D10, D50, and D90 are given in the insets and Table. S1.

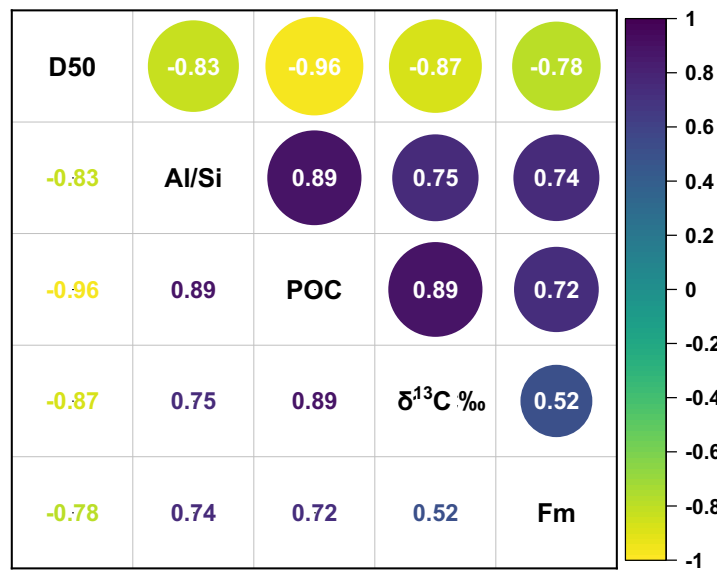


Figure S5. Spearman correlation plot of physical and chemical parameters of SPM in the river cross-section. The size of circles is consistent with the color bar, representing the correlation value.

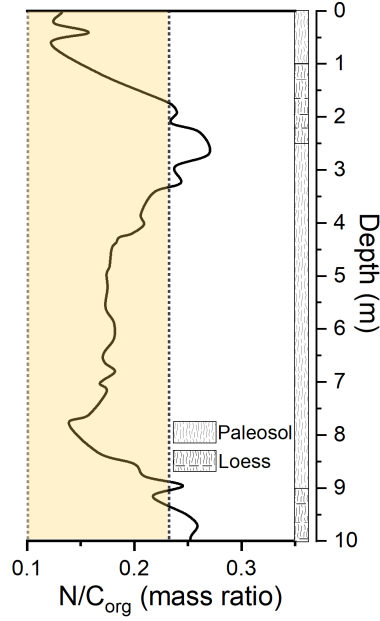


Figure S6. N/C_{org} variations in the Xifeng loess-paleosol sequence with depth (< 10 m), the orange-shaded area constrained by two dotted lines is the range of N/C_{org} (0.10 - 0.23) in SPM (suspended particulate matter) collected from the lower reaches of the Yellow River (data compiled from this study, Yu et al. (2019b), Ran et al. (2013)). N/C_{org} values with the loess-paleosol sequence are from Ning et al. (2006).

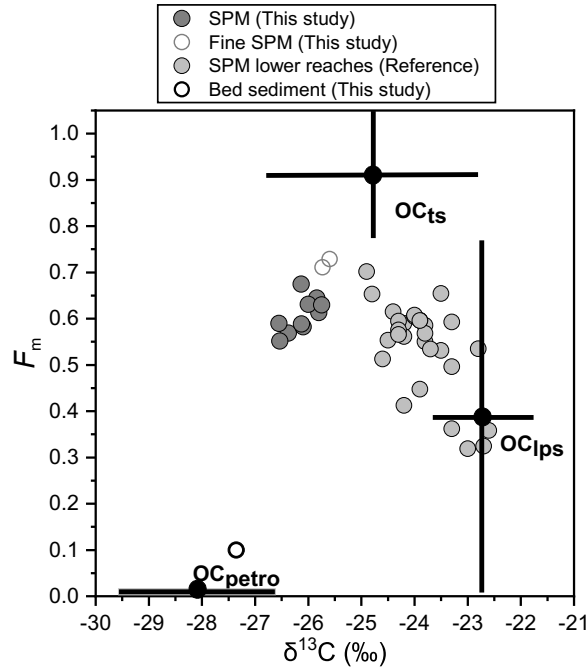


Figure S7. End member mixing space for source provenance of particulate organic carbon in the Huanghe. Apportionment for each end member can be found in Appendix A. Reference data source for SPM lower reaches can be found in Table S1. We use the calc_area algorithm from the MixSIAR package in the R environment to calculate the geometric surface area (Brett, 2014, Moore & Semmens, 2008), which is 7.13 SD^2 , end members are distinct from each other.

Table. S1 Grain size parameters D10, D50, D90 of SPM samples over the channel transect.

| Sample ID | D10 μm | D50 μm | D90 μm |
|------------------|-------------------|-------------------|-------------------|
| JB 1-1 | 1.7 | 19.5 | 86.3 |
| JB 1-2 | 2.0 | 23.7 | 100.9 |
| JB 1-3 | 2.5 | 34.5 | 122.8 |
| JB 2-1 | 2.7 | 39.8 | 119.9 |
| JB 2-2 | 3.8 | 60.4 | 143.0 |
| JB 2-3 | 7.3 | 86.0 | 166.7 |
| JB 3-1 | 3.7 | 50.1 | 108.2 |
| JB 3-2 | 8.5 | 73.1 | 138.3 |
| JB 4-1 | 2.1 | 29.0 | 95.2 |
| JB 5-1 | 5.0 | 58.2 | 110.3 |

References

- Bouchez, J., Gaillardet, J., France-Lanord, C., Maurice, L., and Dutra-Maia, P.: Grain size control of river suspended sediment geochemistry: Clues from Amazon River depth profiles, *Geochemistry, Geophysics, Geosystems*, 12, n/a-n/a, <https://doi.org/10.1029/2010gc003380>, 2011.
- Brett, M. T., Resource polygon geometry predicts Bayesian stable isotope mixing model bias, *Marine Ecology Progress Series*, 514: 1-12, <https://doi.org/10.3354/meps11017>, 2014,.
- Garcia, M.: Sedimentation Engineering, American Society of Civil Engineers, (pp. 21-163) <https://doi.org/10.1061/9780784408148>, 2008.
- Ran, L., Lu, X. X., Sun, H., Han, J., Li, R., and Zhang, J.: Spatial and seasonal variability of organic carbon transport in the Yellow River, China, *Journal of Hydrology*, 498, 76–88, <https://doi.org/10.1016/j.jhydrol.2013.06.018>, 2013.
- Rouse, H.: Modern Conceptions of the Mechanics of Fluid Turbulence, *Transactions of the American Society of Civil Engineers*, 102, 463–505, <https://doi.org/10.1061/TACEAT.0004872>, 1937.
- 2018 River Sediment Bulletin of China, Ministry of Water Resources of the People's Republic of China, http://www.mwr.gov.cn/sj/tjgb/zghlnsgb/201906/t20190618_1342326.html
- Moore, J. W., and Semmens, B. X.: Incorporating uncertainty and prior information into stable isotope mixing models. *Ecology Letters*, 11(5), 470-480, <https://doi.org/10.1111/j.1461-0248.2008.01163.x>, 2008.
- Ning, Y., Liu, W., and An, Z.: Variation of soil $\delta^{13}\text{C}$ values in Xifeng loess-paleosol sequence and its paleoenvironmental implication, *Chinese Science Bulletin*, 51, 1350–1354, <https://doi.org/10.1007/s11434-006-1350-7>, 2006.
- Yu, M., Eglinton, T. I., Haghipour, N., Montluçon, D. B., Wacker, L., Wang, Z., Jin, G., and Zhao, M.: Molecular isotopic insights into hydrodynamic controls on fluvial suspended particulate organic matter transport, *Geochimica et Cosmochimica Acta*, 262, 78–91, <https://doi.org/10.1016/j.gca.2019.07.040>, 2019b.